OpenFOAM 1
COE 347: Computational Fluid Dynamics

Jason Lee, Marco Obregon, Ganesh Somashekhar, Vignesh Winner

February 12, 2026

1 Nondimensional Governing Equations

We consider the steady, incompressible Navier–Stokes equations with constant fluid properties. Let L denote the cavity wall length and U the lid velocity. The fluid has constant density ρ and dynamic viscosity μ. Pressure is scaled using the dynamic pressure level.

Reference Scales

- Length scale: L
- Velocity scale: U
- Pressure scale: ρU^2

Define the nondimensional variables

$$\tilde{x} = \frac{x}{L}, \quad \tilde{y} = \frac{y}{L}, \quad \tilde{u} = \frac{u}{U}, \quad \tilde{v} = \frac{v}{U}, \quad \tilde{p} = \frac{p}{\rho U^2}$$

Nondimensional Continuity Equation

For two dimensional incompressible flow, the continuity equation reduces to

$$\frac{\partial u}{\partial x} + \frac{\partial v}{\partial y} = 0$$

After substituting the nondimensional variables and simplifying, the nondimensional continuity equation becomes

$$\frac{\partial \tilde{u}}{\partial \tilde{x}} + \frac{\partial \tilde{v}}{\partial \tilde{y}} = 0$$

Nondimensional Momentum Equations

Neglecting body forces and writing the steady two dimensional momentum equations component wise yields

x momentum equation

$$\tilde{u}\frac{\partial \tilde{u}}{\partial \tilde{x}} + \tilde{v}\frac{\partial \tilde{u}}{\partial \tilde{y}} = -\frac{\partial \tilde{p}}{\partial \tilde{x}} + \frac{1}{Re}\left(\frac{\partial^2 \tilde{u}}{\partial \tilde{x}^2} + \frac{\partial^2 \tilde{u}}{\partial \tilde{y}^2}\right)$$

y momentum equation

$$\tilde{u}\frac{\partial \tilde{v}}{\partial \tilde{x}} + \tilde{v}\frac{\partial \tilde{v}}{\partial \tilde{y}} = -\frac{\partial \tilde{p}}{\partial \tilde{y}} + \frac{1}{Re}\left(\frac{\partial^2 \tilde{v}}{\partial \tilde{x}^2} + \frac{\partial^2 \tilde{v}}{\partial \tilde{y}^2}\right)$$

Thus, the nondimensional system consists of three equations in three unknowns, the nondimensional velocities and nondimensional pressure.

Nondimensional Number and Physical Interpretation

The only nondimensional parameter that appears in the nondimensional momentum equations is the Reynolds number

$$Re = \frac{\rho U L}{\mu}$$

The Reynolds number represents the ratio of inertial forces to viscous forces in the flow. When Reynolds number becomes very large, viscous effects are small compared to inertial effects and the viscous diffusion terms become negligible, and the momentum equations approach the inviscid Euler form. When Reynolds number becomes very small, viscous effects dominate and inertial terms are weak, and the equations reduce toward the Stokes or creeping flow approximation.

2 Description of Flow, $Re = 10$

The following contour plots were generated in ParaView from the converged solution at $t = 0.5\,\text{s}$ for the 20×20 mesh. A 2D slice was created at $z = 0.005\,\text{m}$ to visualize the flow field.

Contour Lines for U_x

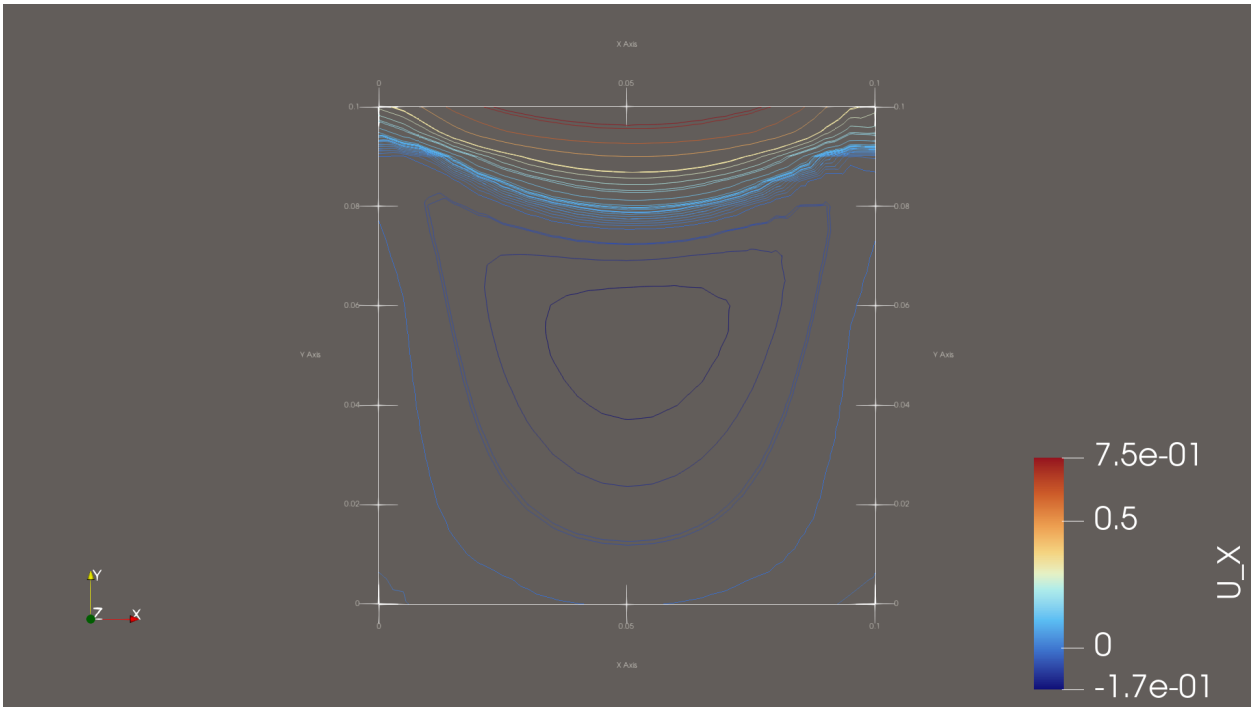

Figure 1: Contour lines for U_x at $Re = 10$.

Contour Lines for U_y

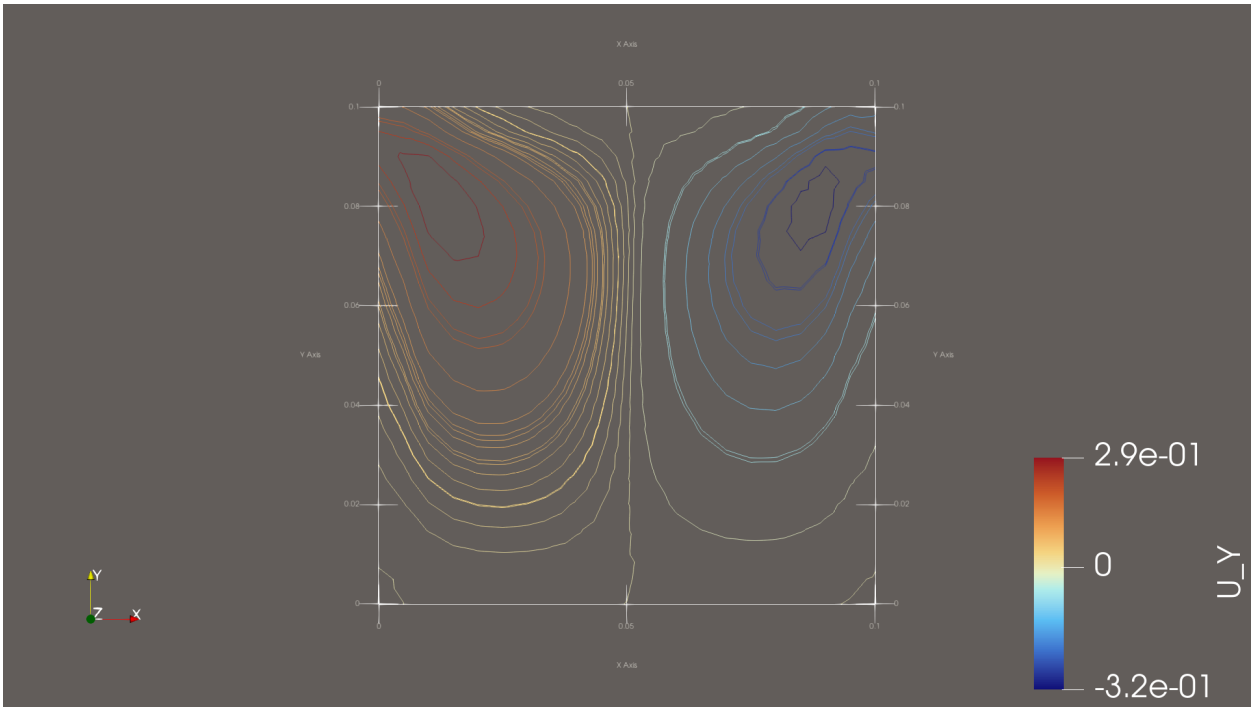

Figure 2: Contour lines for U_y at $Re = 10$.

Velocity Profiles Along the Cavity Centerline

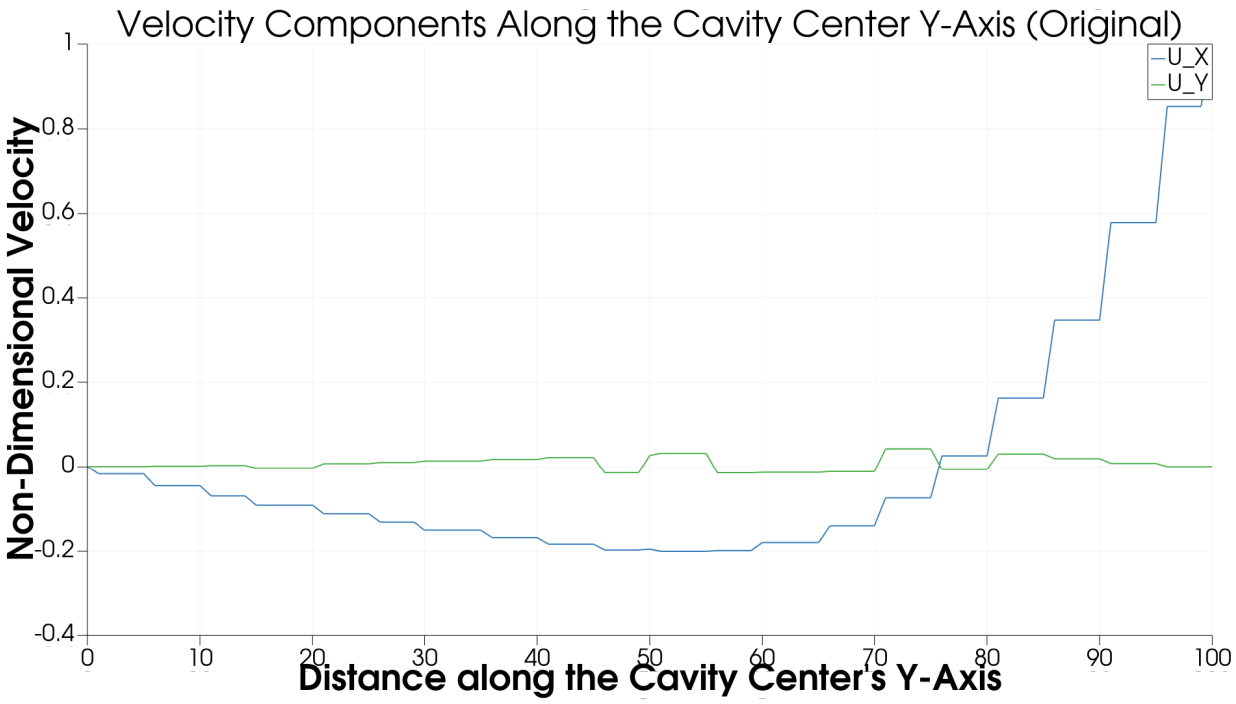

Figure 3: Velocity components along the cavity centerline for the original 20×20 mesh.

Keep in mind that for this graph and all the following u and v graphs, we used default velocity, but they still represent the nondimensional velocity. This is because the reference velocity $U = 1\,\mathrm{m/s}$ and reference length $L = 0.1\,\mathrm{m}$ were chosen for nondimensionalization. When dividing dimensional velocities by $U = 1\,\mathrm{m/s}$, the numerical values remain unchanged, $\tilde{u} = u$ and $\tilde{v} = v$. Similarly, the nondimensional coordinate $\tilde{y} = y/0.1$ scales the y axis from $0.1\,\mathrm{m}$ to a range of 0 to 1, but the shape and physics of the velocity profiles remain identical.

3 Refining the Solution

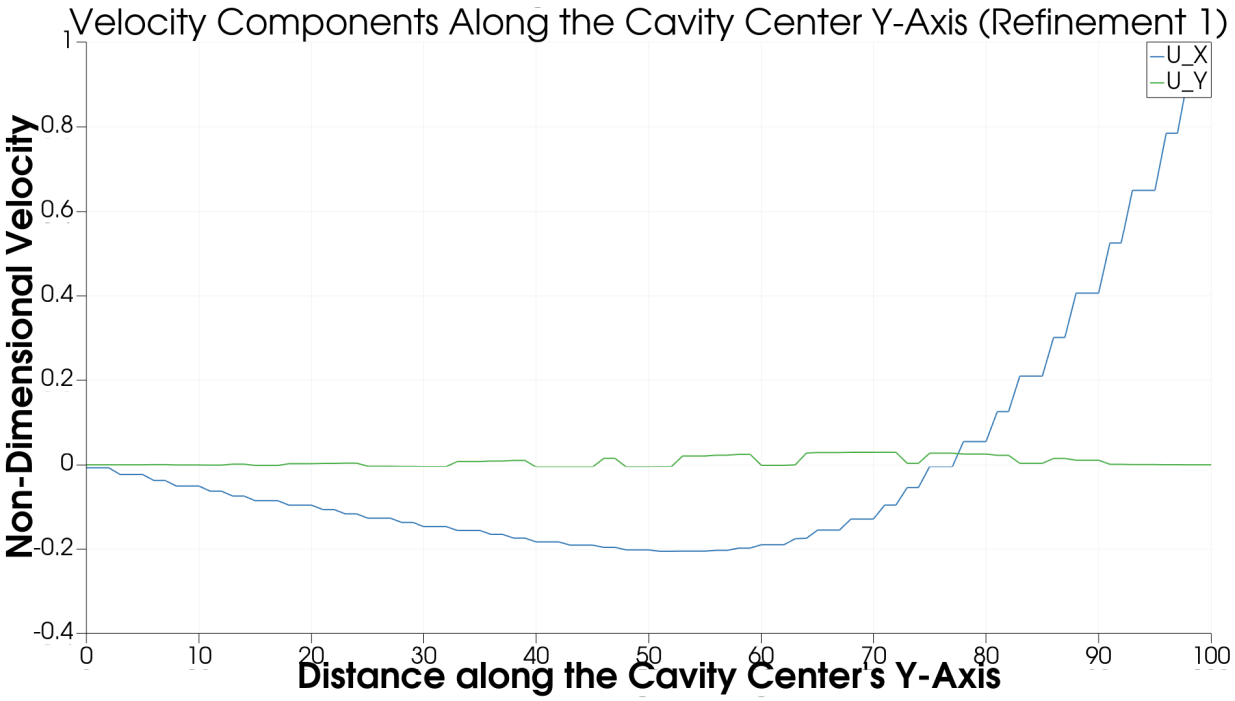

Figure 4: Velocity components along the cavity centerline for refinement 1, 40×40 mesh.

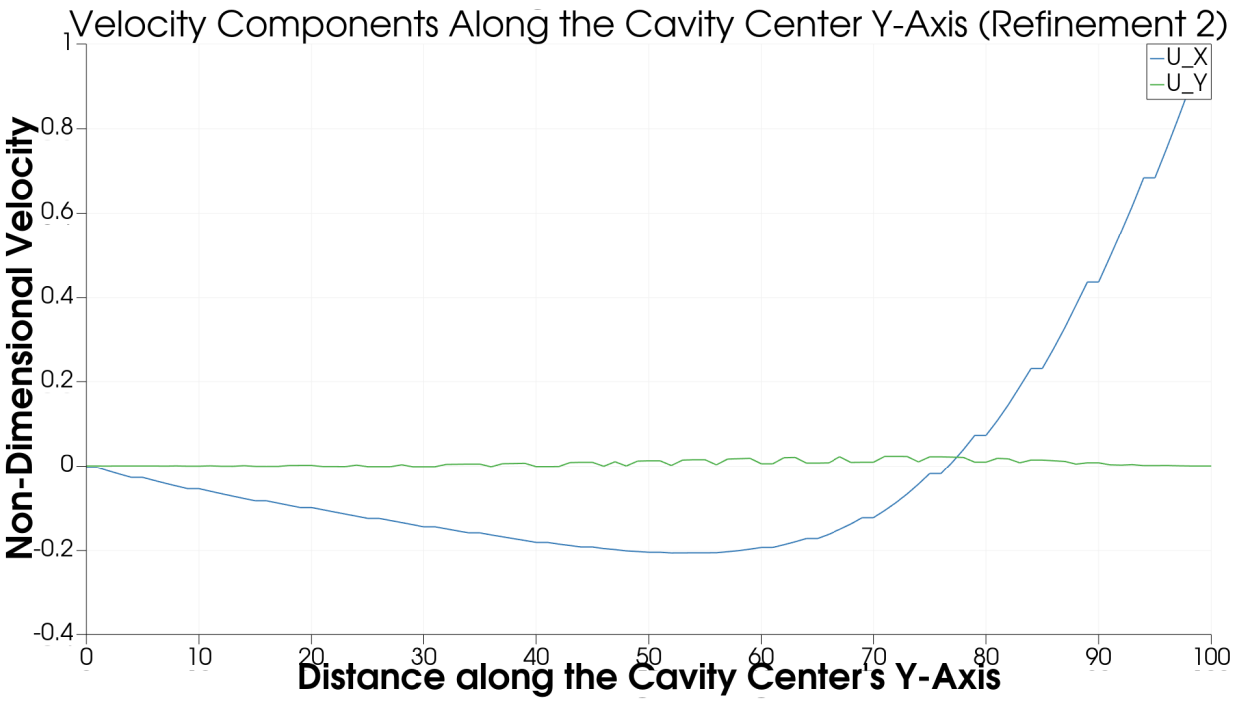

Figure 5: Velocity components along the cavity centerline for refinement 2, 80×80 mesh.

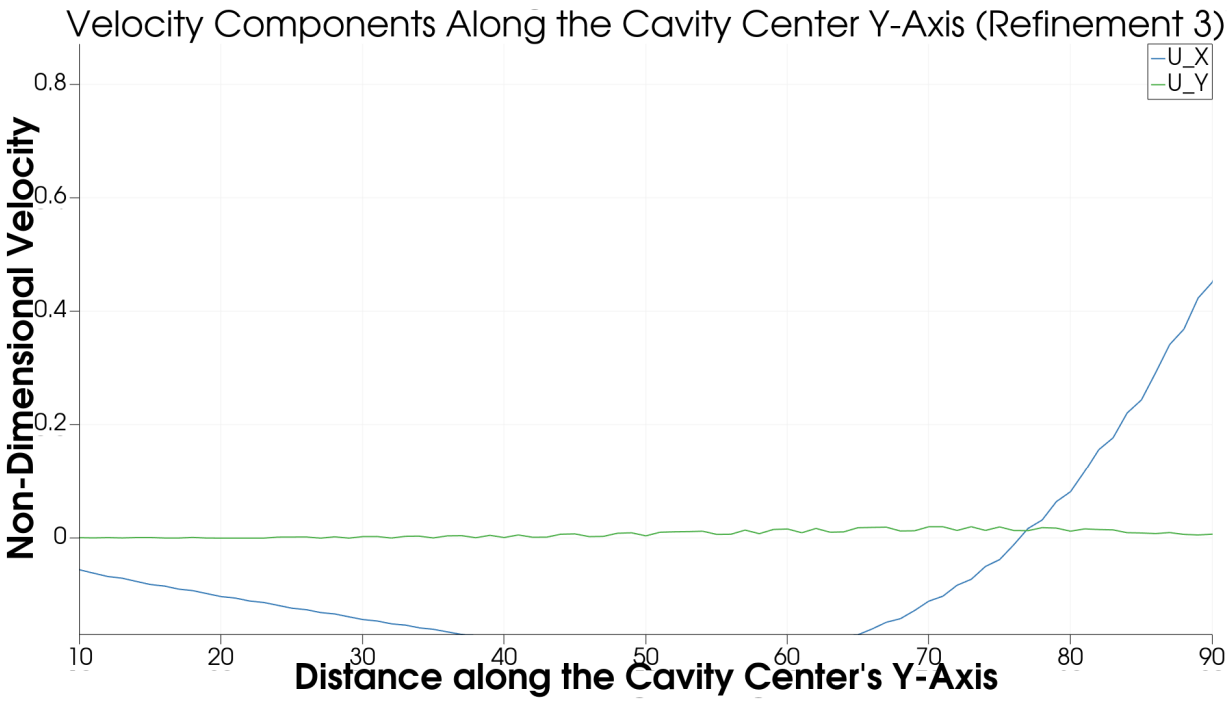

Figure 6: Velocity components along the cavity centerline for refinement 3, 160×160 mesh.

4 Comparison of Velocity Profiles Across Mesh Refinements

Figures show the nondimensional velocity profiles along the vertical centerline, $\tilde{x} = 0.5$, for four mesh resolutions, 20×20, 40×40, 80×80, and 160×160 cells. As the mesh is refined, the velocity profiles become progressively smoother and more accurate. The coarsest mesh exhibits a stepped, blocky appearance, particularly near the moving lid where velocity gradients are steepest. With each refinement, these step like artifacts diminish significantly. The 160×160 mesh produces nearly smooth, continuous profiles, indicating the solution is approaching mesh independence. The most significant improvements occur in high gradient regions, near the moving lid for u velocity and in the recirculation zones where v velocity changes sign. This demonstrates that adequate spatial resolution is critical for accurately capturing flow features in CFD simulations.

Computational Cost

$$C = \frac{\text{Wallclock Time}}{\text{Total Steps}}$$

Case	Grid	N (cells)	Wallclock Time (s)	C (s per step)
cavity_Re10	20×20	400	0.14	0.0014
cavity_Re10_40	40×40	1600	0.58	0.0029
cavity_Re10_80	80×80	6400	5.91	0.0148
cavity_Re10_160	160×160	25600	90.64	0.1133

Table 1: Computational cost per step for each mesh refinement.

5 Computational Cost Scaling Analysis

The wallclock time per step, C, was computed for each mesh refinement and plotted against the total number of cells, N, on a log log scale. A power law fit to the data yields

$$C = 2.0 \times 10^{-6} \, N^{1.068}$$

with an R^2 value of 0.961, indicating excellent agreement with the power law model. The scaling exponent $\alpha = 1.068$ indicates nearly linear computational cost scaling with mesh refinement. This means that when the mesh is refined by a factor of 2 in each direction, quadrupling the total number of cells, the computational cost per time step increases by approximately $2^{1.068} \approx 2.09$ times. The slight superlinearity is typical for iterative CFD solvers, arising from increased solver iterations required for convergence on finer meshes and less favorable cache performance with larger data sets.

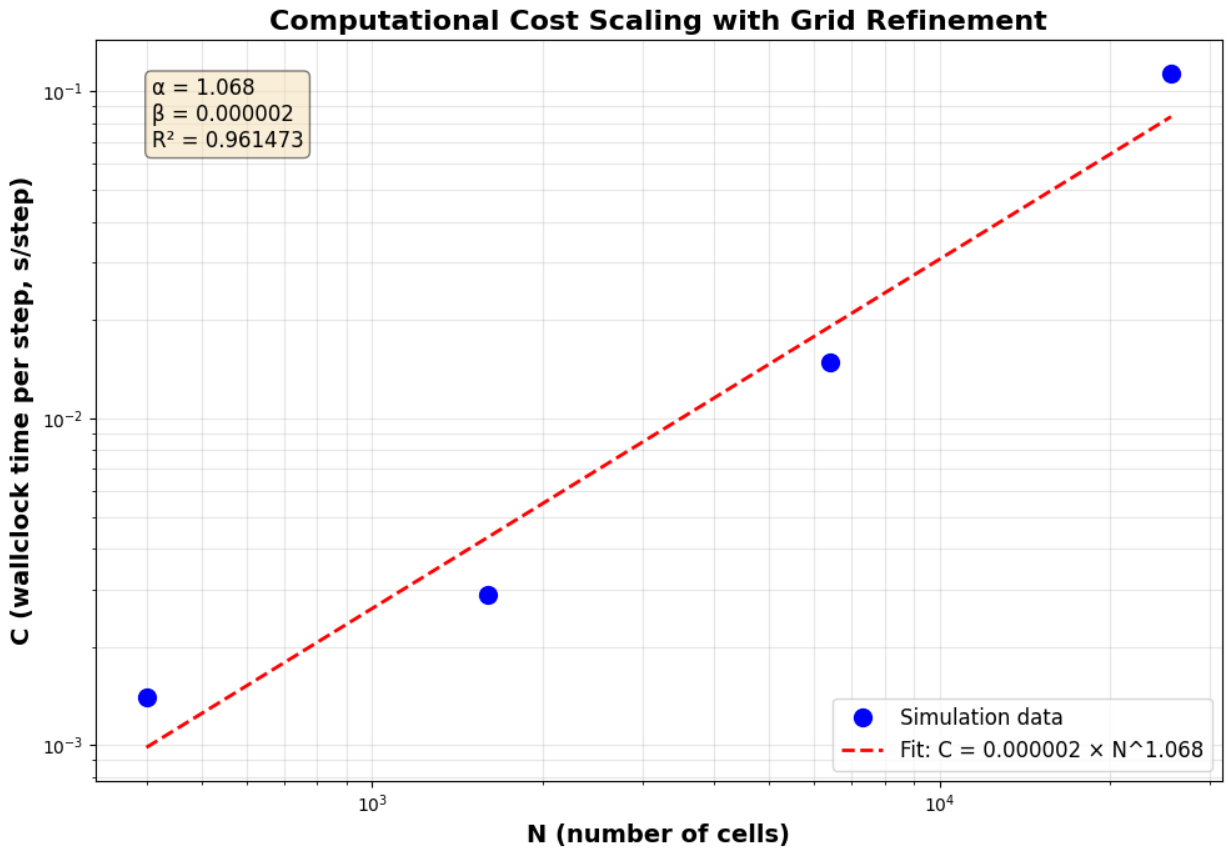

Figure 7: Computational cost scaling with grid refinement on a log log plot.

6 Force on Lid

We computed the nondimensional lid shear stress distribution

$$\tau_e(x) = \left.\frac{\partial u}{\partial y}\right|_{\tilde{y}=1}$$

using the one sided finite difference approach specified in the assignment. In ParaView, we sampled U_x along a line located at the first cell center below the moving lid, $y = L - \Delta y/2$, and evaluated

$$\tau_e(x) \approx \frac{1 - U_{x,P}}{\Delta y/2}$$

This procedure produced $\tau_e(x)$ along the full lid for each Reynolds number case.

τ_e **vs** x

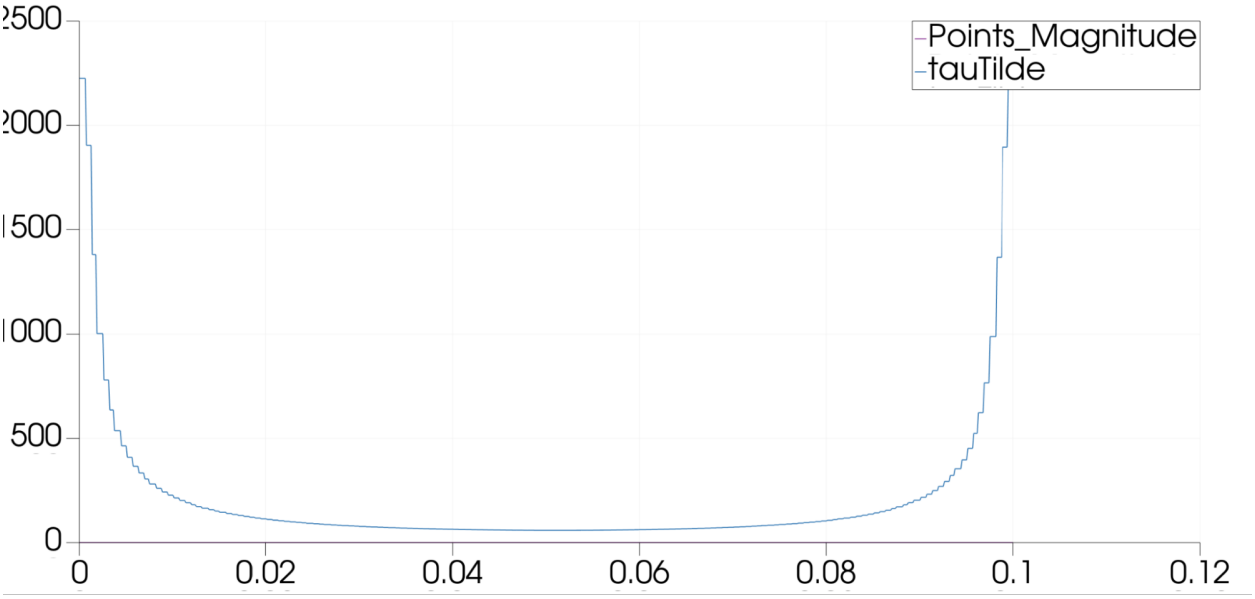

Figure 8: τ_e vs x for $Re = 10$.

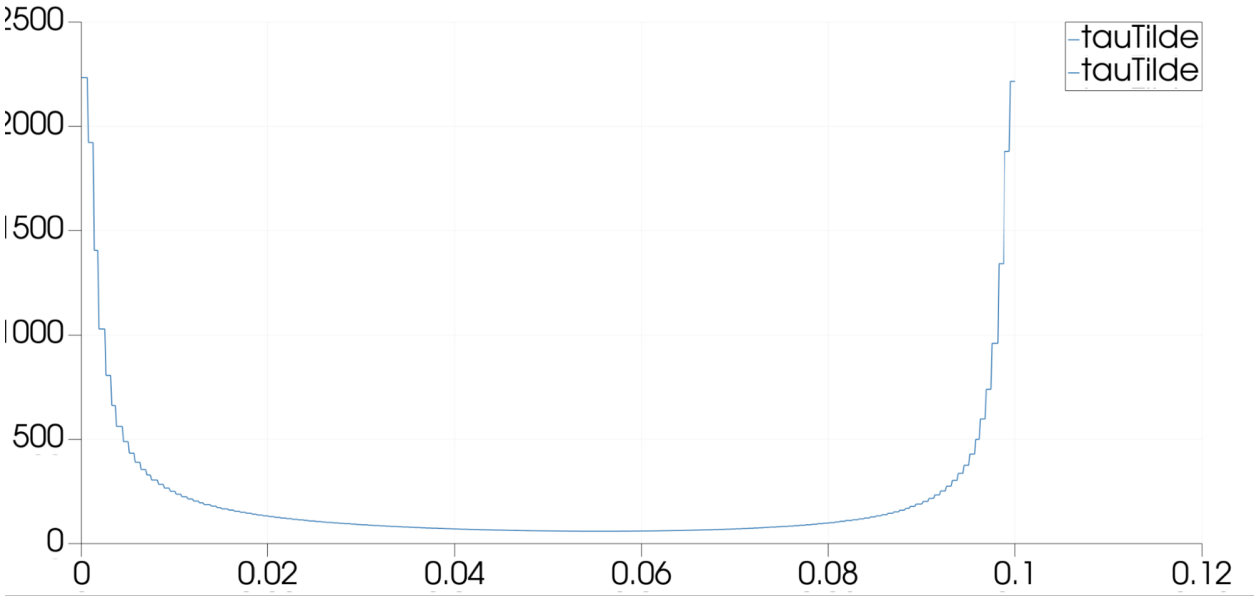

Figure 9: τ_e vs x for $Re = 50$.

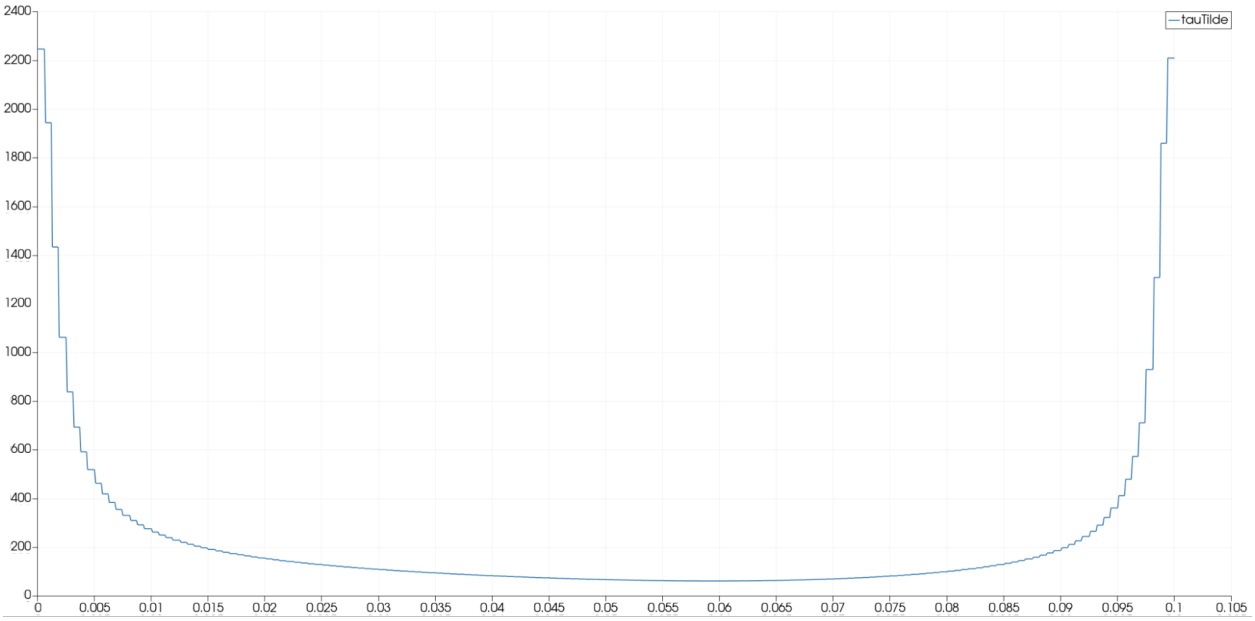

Figure 10: τ_e vs x for $Re = 100$.

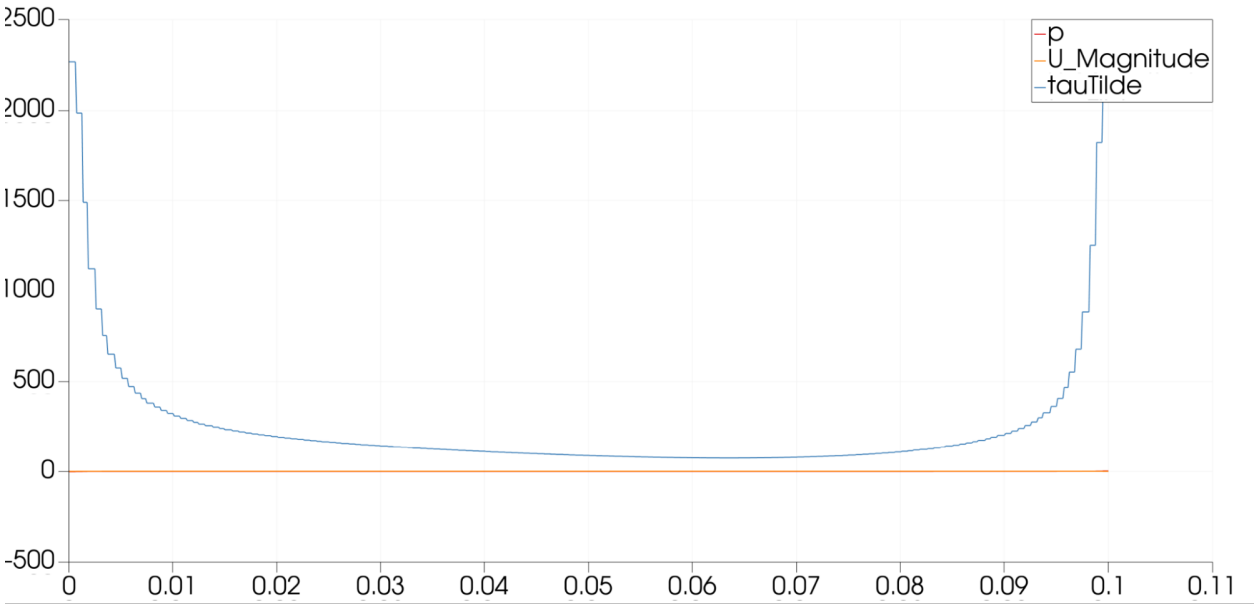

Figure 11: τ_e vs x for $Re = 200$.

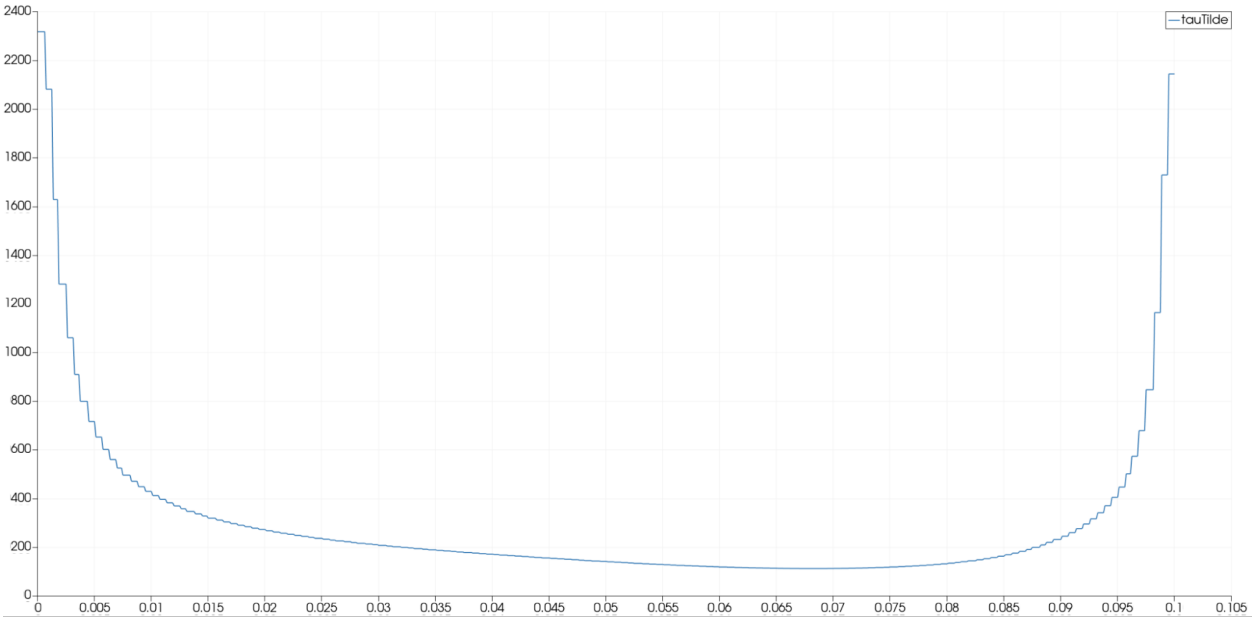

Figure 12: τ_e vs x for $Re = 500$.

The $\tau_e(x)$ distributions show increased shear near the corners, where velocity gradients are strongest. As Reynolds number increases, the corner regions become sharper and more concentrated, consistent with thinning boundary layers and stronger near wall gradients in lid driven cavity flow. As Reynolds number increases, subtle but noticeable changes appear in the $\tau_e(x)$ distributions along the lid. In particular, the right side of the lid exhibits a slight decrease in shear magnitude relative to the lower Reynolds number cases. This behavior is consistent with the development of stronger recirculation and secondary flow structures inside the cavity at higher Reynolds numbers. As inertia becomes more dominant, the primary vortex shifts and strengthens, modifying the velocity gradients near the right corner of the lid. Consequently, while overall integrated shear increases with Reynolds number, the spatial distribution of shear becomes more nonuniform, with localized changes in magnitude near the cavity corners.

From the calculations made for each case, we determine

$$\begin{aligned} Re = 10, &\quad F_e = 21.4016 \\ Re = 50, &\quad F_e = 21.7694 \\ Re = 100, &\quad F_e = 22.7005 \\ Re = 200, &\quad F_e = 24.9029 \\ Re = 500, &\quad F_e = 30.5051 \end{aligned}$$

The nondimensional force on the lid was computed by integrating the lid shear stress distribution,

$$F_e = \int_0^1 \tau_e(x)\, dx$$

as required by the assignment.

We obtained F_e for each Reynolds number from the ParaView integration output and then plotted F_e versus Re on linear and log log axes to evaluate the trend and scaling.

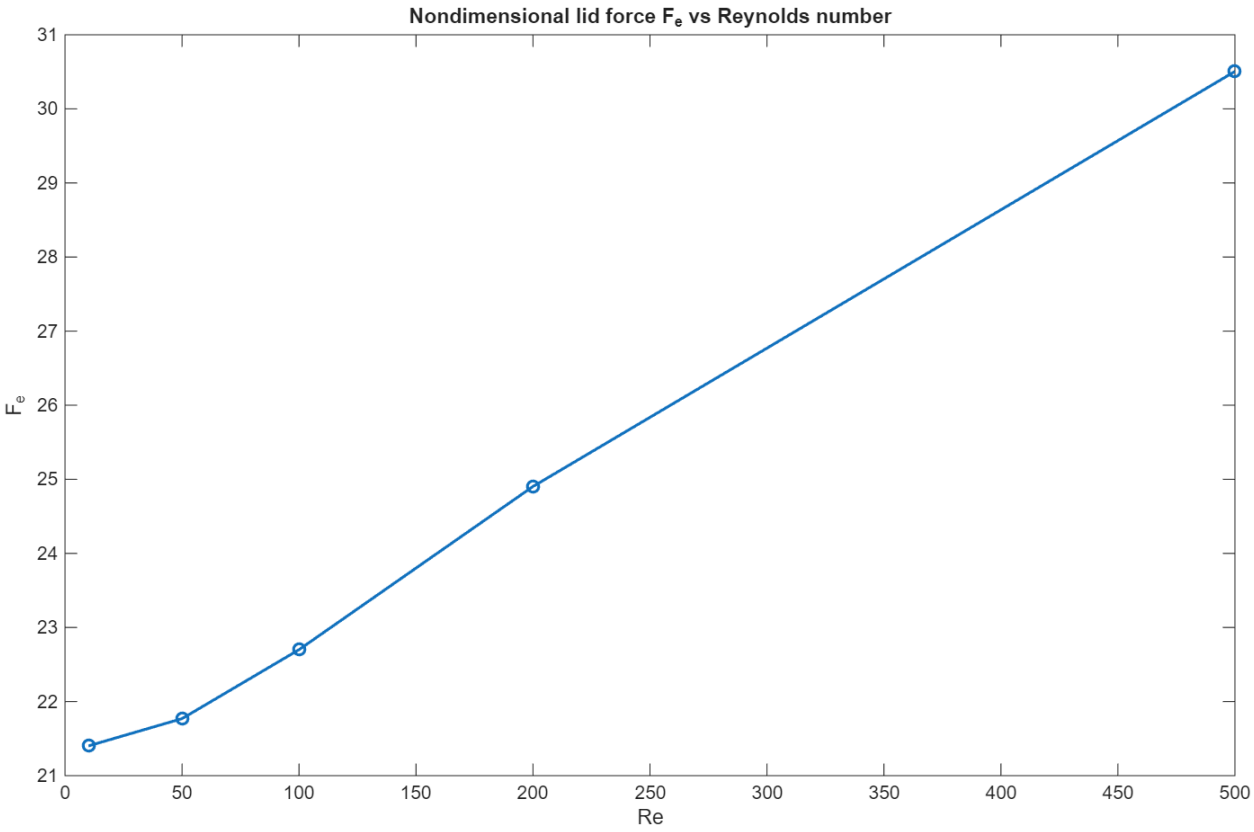

Figure 13: F_e vs Re from Matlab post processing.

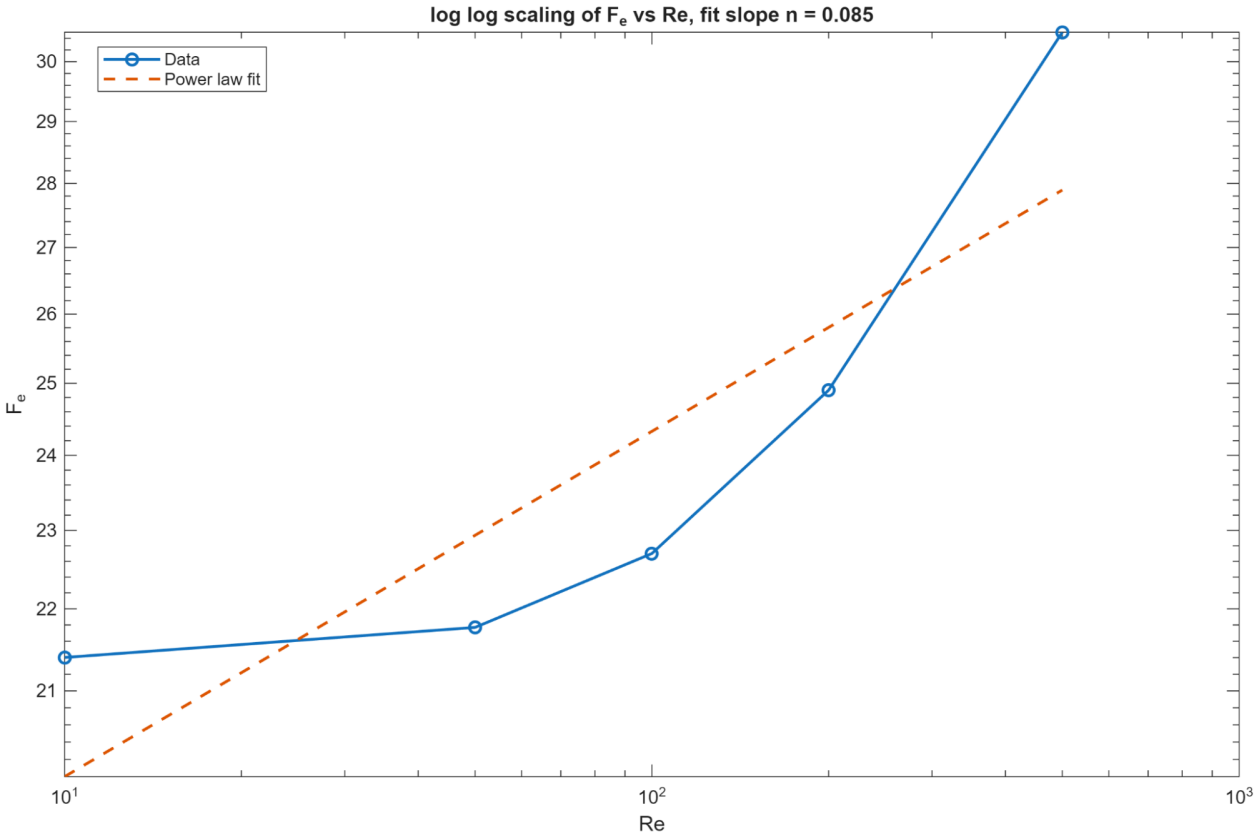

Figure 14: Log log comparison of F_e versus Re.

Across $Re = 10$ to 500, the nondimensional lid force F_e increases with Reynolds number. The growth is driven by stronger velocity gradients near the moving lid and increased shear concentration near the corners as Reynolds number rises. The log log plot summarizes the overall scaling behavior over the simulated Reynolds range.

7. Extra Credit: Aspect Ratio Effects on Lid Force

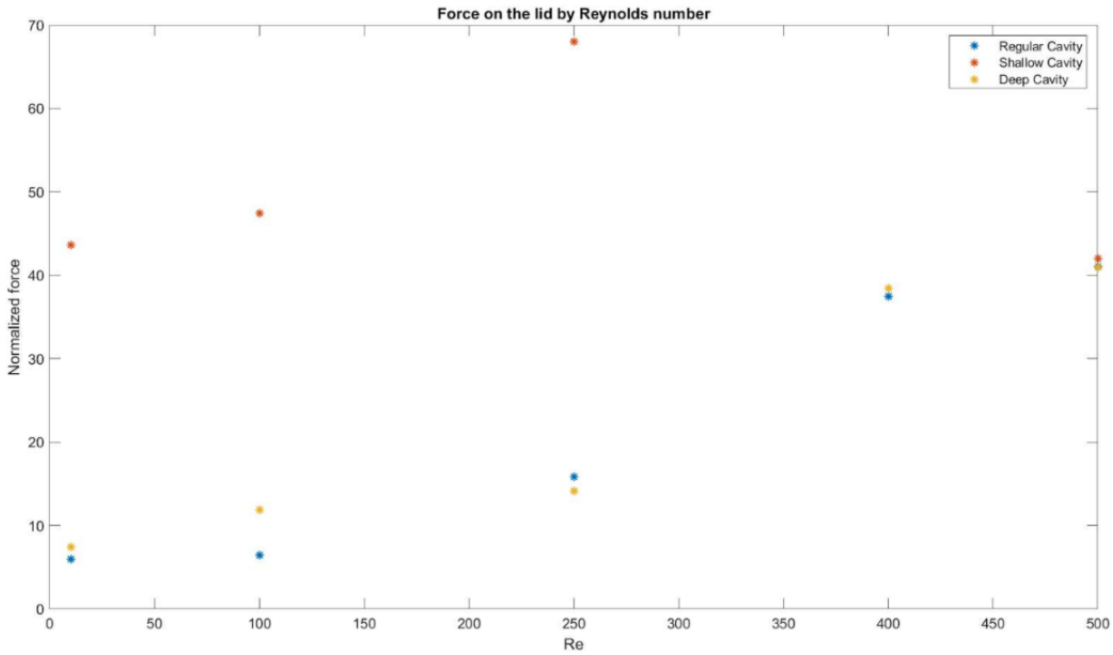

Figure 1: Force on the lid versus Reynolds number for square, shallow ($H/L = 0.5$), and tall ($H/L = 2$) cavities.

The plot of nondimensional lid force versus Reynolds number shows that the force increases steadily as Reynolds number rises up to 500 for all three geometries considered: square, shallow ($H/L = 0.5$), and tall ($H/L = 2$). This overall increase is consistent with stronger velocity gradients and larger shear at the moving lid as inertial effects become more dominant.

However, the cavity aspect ratio produces a noticeable change in magnitude and trend. The shallow cavity produces substantially larger nondimensional force values across the Reynolds number range. This indicates that reducing the cavity height concentrates the recirculating flow closer to the lid, which increases the velocity gradient at the top boundary and therefore raises the shear stress contribution to the integrated lid force.

In contrast, the tall cavity produces force values that remain close to those of the square cavity. With greater vertical space, the primary vortex stretches and distributes momentum over a larger region. This reduces the intensity of the near-lid gradients compared with the shallow case, resulting in a force response similar to the baseline square geometry.

Overall, the results show that decreasing aspect ratio amplifies lid shear and force, while increasing aspect ratio mainly redistributes the flow structure without strongly changing the integrated lid load. This confirms that vertical confinement is a key driver of wall shear behavior in lid-driven cavity flow.